

Response to editor's comments (ms essd-2020-64)

Editor's comments:

"Reader needs to see a much better, more explicit uncertainty analysis. What authors call 'data consistency evaluation' (Section 5) provides good validation, but users should also find detailed informed discussion of uncertainties: instrument uncertainties, performance / deployment uncertainties, environmental (weather, water height) uncertainties, etc. Authors mention many sources of uncertainty (sensor performance, for example) throughout the manuscript but never pull those uncertainties together into a composite uncertainty budget. Figure 3 shows high R2 values for radiation intercomparison, good. Figure 5 shows uncertainty bars but only for the WMO reference stations. Pull this information together into a table of estimated uncertainty by parameter measured, with a short section of author explanations and comments? Data as presented seem to lack any uncertainty, which authors and users will recognize as not plausible."

Response:

Thank you for this suggestion. In response, we have added a Table (Table 5) to summarize the three types of uncertainty. We have added the following passages as explanation:

In section 2.2: "To evaluate the performance of field EC systems, we installed a closed-path EC system (Model CPEC200; Campbell Scientific) at BFG for a brief period in the summer of 2020. The performance uncertainty was based on the difference between the field open-path EC system and this closed-path system. "

In Section 5: "Table 5 is a summary of the uncertainty of key measurement variables at half-hourly intervals. The performance uncertainty is one standard deviation of difference in a variable measured by the field instrument and the same variable measured by a validation instrument (the closed-path EC in the case of eddy fluxes and the laboratory standard radiometer in the case of the radiation fluxes). The environmental uncertainty is one standard deviation of spatial variation of a variable measured at multiple lake sites."

1 **A dataset of microclimate and radiation and energy fluxes from the Lake Taihu Eddy**

2 **Flux Network**

3 Zheng Zhang^{a,b}, Mi Zhang^{a,b,d}, Chang Cao^{a,b}, Wei Wang^{a,b}, Wei Xiao^{a,b,d}, Chengyu Xie^{a,b},
4 Haoran Chu^{a,b}, Jiao Wang^{a,b}, Jiayu Zhao^{a,b}, Lei Jia^{a,b}, Qiang Liu^{a,b}, Wenjing Huang^{a,b},
5 Wenqing Zhang^{a,b}, Yang Lu^{a,b}, Yanhong Xie^{a,b}, Yi Wang^{a,b}, Yini Pu^{a,b}, Yongbo Hu^{a,b}, Zheng
6 Chen^{a,b}, Zhihao Qin^{a,b}, Xuhui Lee^{c*}

7
8 a Yale-NUIST Center on Atmospheric Environment, International Joint Laboratory on
9 Climate and Environment Change (ILCEC), Nanjing University of Information Science and
10 Technology, Nanjing, Jiangsu Province, China

11
12 b Key Laboratory of Meteorological Disaster, Ministry of Education and Collaborative
13 Innovation Center on Forecast and Evaluation of Meteorological Disasters, Nanjing
14 University of Information Science and Technology, Nanjing, Jiangsu Province, China

15
16 c School of Forestry and Environmental Studies, Yale University, New Haven, CT, USA

17
18 d NUIST-Wuxi Research Institute, Wuxi, Jiangsu Province, China

19 * Corresponding author: xuhui.lee@yale.edu

20

21 **Abstract**

22 Eddy covariance data are widely used for the investigation of surface-air interactions.
23 Although numerous datasets exist in public depositories for land ecosystems, few research
24 groups have released eddy covariance data collected over lakes. In this paper, we describe a
25 dataset from the Lake Taihu Eddy Flux Network, a network consisting of seven lake sites and
26 one land site. Lake Taihu is the third largest freshwater lake (area 2,400 km²) in China, under
27 the influence of subtropical climate. The dataset spans the period from June 2010 to
28 December 2018. Data variables are saved as half-hourly averages and include
29 micrometeorology (air temperature, humidity, wind speed, wind direction, rainfall, and
30 water/soil temperature profile), the four components of surface radiation balance, friction
31 velocity, and sensible and latent heat fluxes. Except for rainfall and wind direction, all other
32 variables are gap-filled, with each datapoint marked by a quality flag. Several areas of
33 research can potentially benefit from the publication of this dataset, including evaluation of
34 mesoscale weather forecast models, development of lake-air flux parameterizations,
35 investigation of climatic controls on lake evaporation, validation of remote sensing surface
36 data products, and global synthesis on lake-air interactions. The dataset is publicly available
37 at <https://yncenter.sites.yale.edu/data-access> and from Harvard Dataverse
38 [https://dataverse.harvard.edu/dataset.xhtml?persistentId=doi:10.7910/DVN/HEWCWM&version=DRAFT&fac](https://dataverse.harvard.edu/dataset.xhtml?persistentId=doi:10.7910/DVN/HEWCWM&version=DRAFT&faces-redirect=true)
39 [es-redirect=true](https://dataverse.harvard.edu/dataset.xhtml?persistentId=doi:10.7910/DVN/HEWCWM&version=DRAFT&faces-redirect=true) (Zhang et al., 2020).

40

41

42 **1. Introduction**

43 Inland lakes and reservoirs are a vital freshwater resource for the society. Globally, there are
44 more than 27 million water bodies with size greater than 0.01 km², occupying a total of 3.5%
45 of the Earth's land surface area (Downing et al., 2006; Verpoorter et al., 2014). Accurate
46 observation of the lake microclimate and lake-air interactions will help to better manage this
47 water resource and to better predict how it may be affected by environmental changes.
48 Towards that end, an increasing number of studies have employed the eddy covariance (EC)
49 methodology to monitor physical state (temperature, wind, humidity) and process variables
50 (momentum flux, and radiation and energy fluxes) in the lake environment (Vesala et al.,
51 2006; Blanken et al., 2011; Nordbo et al., 2011; Wang et al., 2014; Li et al., 2015; Yusup and
52 Liu, 2016; Du et al., 2018; Hamdani et al., 2018; Xiao et al., 2018; Wang et al., 2019). Unlike
53 EC studies in land ecosystems, however, data from these lake studies are rarely published as
54 data papers or are archived in public data depositories accessible by the broader scientific
55 community. For example, of the nearly 500 sites that have contributed EC and
56 micrometeorological data to AmeriFlux, a public data depository
57 (<https://ameriflux.lbl.gov/data/data-availability/>), none is a lake site. Although a few
58 scientific groups have provided data supplements to their scientific papers on lake-air fluxes
59 (e. g., Charusombat et al., 2018; Franz et al., 2018; Zhao and Liu, 2018), we are not aware of
60 a data paper devoted to systematic description and archival of EC lake observations.

61
62 In this paper, we describe the dataset from the Lake Taihu Eddy Flux Network (Lee et al.,
63 2014). Established in 2010, the network currently consists of six active lake sites, one

64 inactive lake site, and one active land site. Lake Taihu is the third largest freshwater lake
65 (area 2,400 km²) in China. Data variables are recorded at half-hourly intervals and the
66 measurement has continued for over eight years. Several areas of research can potentially
67 benefit from the publication of this dataset, including evaluation of mesoscale weather
68 forecast models, development of lake-air flux parameterizations, investigation of climatic
69 controls on lake evaporation, validation of remote sensing surface data products, and global
70 synthesis on lake-air interactions.

71

72 This paper is organized as follows. Section 2 is a brief overview of the sites and the
73 instruments used by the network. This is followed, in Section 3, with a description of data
74 quality measures employed during the field monitoring. Section 4 provides the essential
75 information about the dataset, including data variables, gap-filling methods, and data quality
76 flags. Results of post-field evaluation of the data quality are given in Section 5.

77

78 Users of this dataset may be interested in the relevant papers published by our group. Lee et
79 al. (2014) gave an overview of the Lake Taihu Eddy Flux Network. Using the data collected
80 at a subset of the sites and during the early phase of the network, Wang et al. (2014)
81 investigated the spatial variability of energy and momentum fluxes across the lake. Xiao et al.
82 (2013) improved the bulk parameterizations of heat, water and momentum fluxes for shallow
83 lakes. Deng et al. (2013) and Hu et al. (2017) modified the CLM lake simulator (Subin et al.,
84 2012) to improve its prediction of the lake evaporation. Wang et al. (2017) and Zhang et al.
85 (2019b) evaluated the performance of two mesoscale models of the lake-land breeze. More

86 recently, Xiao et al. (2020, manuscript in review) investigated drivers of the interannual
87 variability of the lake evaporation observed at one of the lake sites (BFG). The value of the
88 dataset is enhanced by these peer-reviewed publications because they have helped us to
89 continuously improve our measurement and data processing protocols. For example, we have
90 used the locally-calibrated bulk parameterizations of Xiao et al. (2013) to gap-fill the flux
91 variables.

92

93 **2. Sites and Instrumentation**

94 **2.1 Sites and data periods**

95 Table 1 shows the basic site information and Figure 1 is a map that gives the relative position
96 of Lake Taihu in China and locations of the EC measurement sites. Also shown in Figure 1
97 are WMO baseline weather stations around the lake, whose data can be obtained from
98 National Meteorological Information Center in China (<http://data.cma.cn/site/index.html>).
99 The lake, located between the latitudinal range of 30°5'40" N to 31°32'58" N and
100 longitudinal range of 119°52'32" E to 120°36'10" E, has a total area of 2400 km² and an
101 average depth of 1.9 m. The climate is subtropical monsoon, with an annual mean
102 temperature of 16.2°C and annual total precipitation of 1122 mm. The lake is ice-free
103 throughout the year.

104

105 The EC network consists of seven lake sites and one land site. The lake sites (Meiliangwan
106 (MLW), Dapukou (DPK), Bifenggang (BFG), Xiaoleishan (XLS), Pingtaishan (PTS),
107 Dongtaihu (DTH), Meiliangwan2 (MLW2)) are distributed according to biological

108 characteristics and across eutrophication gradients of the lake. The MLW site, located in
109 Meiliangwan Bay near the north shore of Lake Taihu, was the first site in operation; the
110 measurement began in June 2010 and was replaced by MLW2 in 2018, at 10 km southwest of
111 MLW. Both MLW and MLW2 sites are located in the lake eutrophic zone. BFG is located in
112 the east part of Lake Taihu in relatively clean water inhabited by submerged vegetation with
113 a growth season from April to November. DTH is located in the shallow water (mean depth
114 of 1.3 m) in the southeast part of the lake. After more than 20 years of crab aquaculture, this
115 zone was returned to unmanaged state in December 2018 in order to improve water quality.
116 The observation at DTH enables the examination of lake-air exchange processes in the
117 transition from human management to a natural state. PTS is situated in the middle of Lake
118 Taihu where occasional algal blooms occur and no aquatic vegetation is present. DPK is
119 located near the west shore, in a relatively deep (depth 2.5 m) super eutrophic zone due to
120 heavy influence of agricultural and urban runoffs. XLS is located in the relatively clean and
121 vegetation-free zone in the southeast. Finally, DS is a land site surrounded by rice agriculture,
122 serving as a land reference for the lake sites. The MLW site is situated at a distance of 200 m
123 from the north shore of the lake. All the other lake sites in the lake are at a distance of more
124 than 1 km away from the land.

125
126 The lake water level is monitored daily by the Taihu Basin Authority at five locations around
127 the lake (<http://www.tba.gov.cn/>). Using the water-level time series, we have constructed the
128 water depth for our eddy covariance sites (Figure 2).

129

130 **2.2 Instrumentation**

131 Each site is equipped with an EC system for long-term, continuous monitoring of the surface
132 momentum, sensible heat, latent heat and carbon dioxide fluxes. The EC system consists of a
133 sonic anemometer/ thermometer (Model CSAT3A; Campbell Scientific, Logan, UT, USA)
134 and a CO₂/H₂O infrared gas analyzer (Model 7500A, LI-COR, Inc., Lincoln, NE, USA at DS,
135 MLW, MLW2 and DPK; Model EC150, Campbell Scientific at other sites). The EC system
136 is at a height of 3.5 to 9.4 m above the water surface at the lake sites and at a height of 20 m
137 above the ground at the land site.. Other measurements include air humidity and air
138 temperature (Model HMP45D/HMP155A; Vaisala, Inc, Helsinki, Finland), wind speed and
139 wind direction (Model 03002; R. M. Young Company, Traverse City, MI, USA) and four
140 components of the net radiation (Model CNR4; Kipp & Zonen B. V., Delft, the Netherlands).
141 At the lake sites, water temperature profile was measured with temperature probes (Model
142 109-L; Campbell Scientific) at the water depth of 20, 50, 100, and 150 cm and in the
143 sediment at about 5 cm below bottom of the water column. The top four temperature sensors
144 were tied to a nylon rope hanging from a buoy to ensure that they were at the designed depths
145 regardless of water level fluctuations. At the DS land site, soil temperature profile was
146 measured with the same type of probes at the depths of 5, 10, 20 cm. The MLW and the DS
147 sites are supported by A/C power and other sites are powered by battery packs connected to
148 solar panels. Measurements at the lake sites were made on fixed platforms. Readers are
149 referred to Lee et al. (2014) and Xiao et al. (2017) for photographs of the platform and the
150 instruments.

151

152 All the variables are reported as 30-min averages. The EC data are expressed in the natural
153 coordinate system (Lee et al., 2004). In this coordinate system, the longitudinal coordinate
154 axis is aligned with the 30-min mean velocity vector so that the 30-min mean lateral and
155 vertical velocity components are zero and the magnitude of the mean velocity is equal to the
156 mean longitudinal component, and the covariance between the lateral and the vertical
157 velocity components is zero. Additionally, a small density correction has been applied to the
158 water vapor flux according to Webb et al. (1980).

159

160 —

Formatted: Left

161 **3 Data Quality Control during Field Monitoring**

162 Every site in the Lake Taihu Eddy Flux Network is equipped with a wireless transmission
163 module for real-time monitoring and for data transmission. Time series of all 30-min
164 variables are examined weekly and abnormal behaviors are flagged for site operators. Each
165 site is visited every one to two months to perform instrument repair and maintenance and to
166 download 10 Hz EC data. The data coverage rates are summarized in Table 2, where the
167 percentage values represent the proportions of data with quality flag 0, which indicates
168 high-quality original measurement (Table 3).

169

170 The four-way net radiometers at MLW and XLS were compared in the field against a
171 laboratory standard of the same type in the summer of 2018 to check their long-term stability
172 (Figure 3). These two sites were chosen because they have been in operation for more than
173 five years. Additionally, the radiometer at MLW was relocated to MLW2 after MLW had

174 been discontinued. The laboratory standard, which had been calibrated at the manufacturer
175 prior to this performance evaluation, was mounted next to the field instrument for about 10
176 days at each site, covering overcast to clear-sky conditions. The mean bias error was smaller
177 than 1 W m^{-2} for all the radiation components. It was -0.81, -0.81, 0.79 and -0.44 W m^{-2} for
178 the downward shortwave, upward shortwave, downward longwave and upward longwave
179 radiation flux at MLW, respectively. The corresponding values were 0.91, 0.40, 0.69 and
180 0.77 W m^{-2} for XLS. (Comparison experiments are being planned for the other sites.)

181
182 The EC gas analyzers were calibrated every one to two years. The zero-point calibration was
183 carried out with high-purity nitrogen gas, the CO_2 span calibration was made with standard
184 carbon dioxide gases (in the concentration range of 389 to 525 ppm) provided by the National
185 Institute of Meteorology (NIM), China and certified to an accuracy of 1%, and the H_2O span
186 calibration was made with a portable dew-point generator (LI-610; LI-COR, Inc.).

187

188 **4. Gap-filling Methods and Data Quality Flags**

189 We use five-point moving average to screen outliers. If the deviation from the moving
190 average is greater than two standard deviations, the data point is discarded. If a gap length is
191 30 min to 1 h, the gap is filled by linear interpolation. Larger gaps in meteorological variables,
192 radiation components and water temperature are filled with linear regression involving
193 observation of the same variable at another site. This spatial interpolation consists of three
194 steps. First, linear correlation is calculated using the valid data at the target site and at all
195 other sites for the month during which the data gap occurred. Second, the observation at the

196 site with the highest linear correlation is used to establish a linear regression equation. Third,
197 the gap at the target site is filled with the linear regression and the observation at that site.

198

199 Radiation data gaps at the DS land site require special treatment. The radiometer at DS eddy
200 flux site ended in January 2013. Subsequent measurements of the radiation component are
201 provided by a radiometer belonging to the Dongshan WMO weather station at a distance of
202 50 m from the eddy covariance tower (Figure 1). While large gaps in meteorological
203 variables (air temperature, relative humidity, wind speed and air pressure), downward solar
204 radiation and downward longwave radiation are filled with the spatial interpolation method,
205 large gaps in upward shortwave radiation and upward longwave radiation cannot be filled
206 with data from other lake sites even with linear regression. In the case of the upward
207 shortwave radiation, the data gaps were filled using the relationship between downward
208 shortwave radiation and the monthly mean albedo. In the case of upward longwave radiation,
209 the data gaps were filled by a regression equation between the upward longwave radiation
210 and the fourth power of soil temperature at 5-cm depth. Compared to the original data, the
211 gap-filled data do not capture the full diurnal variations because the 5-cm soil temperature
212 has smaller diurnal amplitudes than the soil surface temperature, but the daily-mean upward
213 longwave radiation flux seems reasonable.

214

215 Large data gaps in the EC variables (sensible heat flux, latent heat flux and friction velocity)
216 are filled with a hybrid method. First, if observations exist for the relevant state variable, the
217 gap is filled with the bulk transfer relationship using a transfer coefficient tuned locally for

218 each site (Xiao et al., 2013). For example, the relationship for filling gaps in the sensible heat
219 flux is

$$220 \quad H = \rho_a c_p C_H U (T_s - T_a)$$

221 where ρ_a is air density, c_p is specific heat of air at constant pressure, C_H is the transfer
222 coefficient for sensible heat, T_a is air temperature and T_s is water surface temperature. The
223 transfer coefficient C_H is determined from the observed H and the state variables (U , T_a and
224 T_s) outside gap periods. The missing data on H is then filled with the above relationship using
225 the tuned C_H the observed U , T_a and T_s . Second, if data for the state variable is missing, the
226 spatial interpolation method is used to fill the gaps in these EC variables.

227
228 The spatial interpolation method described above occasionally causes a sudden jump at the
229 beginning or end of a data gap. To harmonize the data, we apply a 5-point moving averaging
230 to the gap-filled time series. If a data point deviates by 2 times of the standard deviation from
231 the moving average, it is replaced by linear interpolation using the two adjacent data points.

232
233 Each data variable is assigned a quality flag to distinguish original measurements and
234 gap-filled values and gap-filling methods (Table 3). The data flags employed here should not
235 be confused with quality flags commonly assigned to the EC methodology in the literature.
236 Specifically, Flag 0 indicates high-quality original data. Other flag values indicate gap-filled
237 data or missing values. Flag 1 indicates that the data was filled by temporal interpolation.
238 Flag 2 indicates that the data was filled by the spatial interpolation method. Flag 3 for the EC
239 variables indicates that the data was filled by the bulk relationship. We also use Flag 3 to

240 mark the upward shortwave and longwave radiation data filled with the albedo and the
241 surface temperature relationship, respectively, for the DS land site. Missing values occur on
242 some situations, which are marked with Flag 4. Figure 4 is an example showing the gap-filled
243 time series of several variables at BFG along with the flag status.

244

245 Rainfall data has not been quantity-controlled or gap-filled. Because of the episodic nature of
246 rainstorms and high spatial variability of rainfall, it is not appropriate to fill data gaps with
247 the time or spatial interpolation method. The total rain amount is likely biased low because
248 no wind screens are used to protect the rain gages from the influence of wind which is much
249 higher on the lake than on land (Figure 5 below). On several site visits, the drain opening to
250 the tipping bucket was found to be partially blocked by debris. Rain amount at a constant and
251 low rate and excessively long rain duration are evidence of such blockage. The flag status of
252 0 for the rainfall variable simply indicates that the field measurement is available, but it does
253 not guarantee high data quality.

254

255 The data coverage begins from the start time of each site (Table 1) and ends in December
256 2018. The time resolution is 30 min. The dataset includes microclimate variables (air pressure,
257 air temperature, relative humidity, wind speed, wind direction and rainfall), radiation fluxes
258 (upward and downward shortwave radiation, upward and downward longwave radiation),
259 water temperature at depth of 0.2 m, 0.5 m, 1.0 m and 1.5 m, and in the 5-cm sediment) and
260 eddy fluxes (friction velocity, sensible heat and latent heat fluxes; Table 4). The time stamp is
261 Beijing time (UTC + 8 h) given by data columns 1 to 5 as year, month, day, hour, and minute,

262 and marks the end of the observation period. For example, time stamp “2012, 1, 1, 12, 00”
263 indicates that the data acquisition period is from 11:30 to 12:00 on January 1, 2012.

264

265 Although the data table does not include the radiative surface temperature T_s , the user can
266 easily calculate it from the two longwave radiation fluxes, as

267
$$T_s = \left(\frac{L_{\uparrow} - (1 - \varepsilon)L_{\downarrow}}{\varepsilon\sigma} \right)^{\frac{1}{4}}$$

268 where σ is the Stefan-Boltzmann constant, ε is emissivity, and L_{\uparrow} and L_{\downarrow} are upward and
269 downward longwave radiation flux, respectively. We use a value of 0.97 for lake surface
270 emissivity in this calculation (Deng et al., 2013; Wang et al., 2014).

271

272 5. Data Consistency Evaluation

273 Figure 5 compares the annual mean air temperature, relative humidity, and wind speed at the
274 Taihu eddy flux sites with those at the four WMO weather stations (Wuxi, Liyang, Huzhou
275 and Dongshan) around the lake (Figure 1). The error bars represent the maximum and
276 minimum values among the four WMO stations and the lines represent the mean values of
277 the four station measurements. The annual mean air temperature at DTH is 0.3°C higher than
278 the station mean. At other sites, air temperature is in close agreement of the weather station
279 data, in terms of both magnitude and inter-annual variability. The annual mean wind speed at
280 MLW, a site near the shoreline, is comparable with the station data. At other more exposed
281 sites, the wind speed is much higher than observed at the WMO stations. The annual mean
282 relative humidity RH shows a larger spread among the eddy flux sites than among the WMO

283 stations partly because the measurement height at the eddy flux sites is not standardized
284 (Table 1). The upward trends in RH over time at DPK and XLS seem to be related more to
285 aging of the sensor than to a real inter-annual variability. We have not fully investigated this
286 aging problem, but it is possible to rectify it by doing a detailed regression analysis against
287 the station data.

288
289 Consistency of the energy flux variables can be evaluated with the energy balance closure.
290 Using observations made at a subset of the sites in the earlier years of the flux network,
291 Wang et al. (2014) reported a closure rate of 70 % to 110 % on the monthly basis, meaning
292 that the sum of the measured monthly sensible and the latent heat flux $H + \lambda E$ is 70 % to
293 110 % of the monthly available energy $R_n - G$, where R_n is net radiation and G is heat storage
294 in the water column. By selecting days without data gaps, we found that the daily energy
295 balance closure is in the range between 66 % and 78 % for all the lake sites and all the years.
296 Such closure rates are typical of eddy covariance observations (Tanny et al., 2008; Wilson et
297 al., 2002).

298
299 We have shown that the monthly latent heat flux at the lake sites MLW, BFG and DPK
300 during July 2010 to August 2012 follows the Priestley-Taylor (PT) model prediction with the
301 original PT constant α of 1.26 and that at the DS land site is in agreement with the PT model
302 if the constant is lowered to 1.0 (Lee et al., 2014). Figure 6 demonstrates that the same
303 relationships hold for all the sites and all the observational months, indicating the overall
304 stability of our measurement systems and the robustness of our gap-filling procedure. The

305 reader is reminded that the monthly latent heat flux in Figure 6 has been adjusted to force
306 energy closure following the method recommended by Barr et al. (1994), Blanken et al.
307 (1997) and Twine et al. (2000). (The half-hourly flux data in the data archive have not been
308 adjusted for energy balance.)

309

310 The Stefan-Boltzmann Law offers another way for checking data consistency. Because the
311 lake surface emits longwave radiation like a blackbody and because the annual mean air
312 temperature and the surface water temperature are nearly identical at this lake (Wang et al.,
313 2014), the change in the annual upward longwave radiation ΔL_{\uparrow} can be expressed as

$$314 \quad \Delta L_{\uparrow} = 4\sigma T_a^3 \Delta T_a$$

315 where T_a is annual mean air temperature, and Δ is the difference between the target year and
316 the year with the lowest air temperature observed at the site. All the five long-term lake sites
317 show good consistency between the longwave radiation and the air temperature observations
318 (Figure 7).

319

320 Table 5 is a summary of the uncertainty of key measurement variables at half-hourly intervals.

321 The performance uncertainty is one standard deviation of difference in a variable measured

322 by the field instrument and the same variable measured by a validation instrument (the

323 closed-path EC in the case of eddy fluxes and the laboratory standard radiometer in the case

324 of the radiation fluxes). The environmental uncertainty is one standard deviation of spatial

325 variation of a variable measured at multiple lake sites.

326

327 **6 Data availability**

328 All data can be open-accessed online for download and use at <https://yncenter.sites.yale.edu/>
329 and from Harvard Dataverse (<https://doi.org/10.7910/DVN/HEWCWM>, Zhang et al., 2020).

330

331 **7 Summary**

332 The dataset described here consists of microclimate variables (air temperature, air humidity,
333 wind speed, wind direction, water or soil temperature profile, and rainfall), four components
334 of the radiation balance, friction velocity, and sensible and latent heat fluxes observed at
335 seven lake sites and one land site. The period of coverage is from June 2010 to December
336 2018. The observation interval is 30 min. Except for rainfall and wind direction, all other
337 variables have been gap-filled. Every data point is tagged with a data quality flag to help the
338 user determine how to best use the data.

339

340 **Author contribution**

341 XL, WX and MZ directed the field program, ZZ performed data gap-filling and prepared the
342 data for public release, CC, WW, CX, HC, JW, JZ, LJ, QL, WH, WZ, YL, YX, YW, YP, YH,
343 ZC and ZQ participated in field data collection, and ZZ, XL and MZ wrote the manuscript.

344

345 **Competing interests**

346 The authors declare no conflict of interest.

347

348 **Acknowledgments**

349 This work was supported by the National Key R&D Program of China (to MZ, CC, WW &
350 WX; grant number 2019YFA0607202), the National Natural Science Foundation of China (to
351 MZ, WW & WX; grant numbers 41575147, 41801093, and 41475141) and the Priority
352 Academic Program Development of Jiangsu Higher Education Institutions (to WX; grand
353 number PAPD).

354

355

356

357

358 **Table 1.** A list of sites in the Lake Taihu Eddy Flux Network

Site ID	MLW	DPK	BFG	XLS	PTS	MLW2	DTH	DS
Lat (°N)	31.4197	31.2661	31.1685	30.9972	31.2323	31.3818	31.0611	31.0799
Long (°E)	120.2139	119.9312	120.3972	120.1344	120.1086	120.1608	120.4704	120.4346
Start date	Jun 2010	Aug 2011	Dec 2011	Nov 2012	Jun 2013	Feb 2018	Nov 2017	Apr 2011
Biology	Eutrophic	Super eutrophic	Submerged macrophyte	Transitional	Mesotrophic	Eutrophic	Aquaculture	Cropland/ Rural residence
Met height (m)	3.5	8.0	8.5	9.4	8.5	6.0	4.5	10.0
T _w / T _s depths (cm)	20, 50, 100, 150, sediment	20, 50, 100, 150, sediment	20, 50, 100, 150, sediment	20, 50, 100, 150, sediment	20, 50, 100, 150, sediment	20, 50, 100, 150, sediment	20, 50, sediment	5, 10, 20
Radiation height (m)	1.5	1.5	1.5	1.5	1.5	1.5	1.5	3.0
EC height (m)	3.5	8.5	8.5	9.4	8.5	6.0	4.5	20

359

360

361

362 **Table 2.** Percent of data coverage. The percentage represents the proportion of high-quality
363 original measurement.

Variable type	MLW	DPK	BFG	XLS	PTS	DTH	MLW2	DS
Micrometeorology	93.3	81.1	97.6	97.0	97.5	98.1	90.3	91.7
Radiation flux	85.5	90.8	96.9	97.4	98.6	98.2	98.2	82.7
Water/soil temperature	83.4	81.3	94.0	91.1	90.3	87.7	22.4	98.4
Eddy flux	73.3	61.8	82.7	79.1	80.6	85.7	85.5	82.8

364

365

366

367

368

369 **Table 3.** A list of data quality flags

Flag	Data quality description
0	Original data
1	Gap-filled with time interpolation
2	Gap-filled with spatial interpolation
3	Gap-filled with bulk relationship
4	NAN

370

371

373 **Table 4.** A list of data columns and variable definitions

Column	Description	Variable name	Unit
1	Year	Year	–
2	Month	Month	–
3	Day	Day	–
4	Hour	HH	–
5	Minute	MM	–
6	Day of Year	DOY	–
7	Air pressure	P	kPa
8	Quality flag of air pressure	P_flag	
9	Air temperature	Ta	°C
10	Quality flag of air temperature	Ta_flag	
11	Relative humidity	RH	%
12	Quality flag of Relative humidity	RH_flag	
13	Wind speed	WS	m s ⁻¹
14	Quality flag of wind speed	WS_flag	
15	Wind direction	WD	Degree
16	Quality flag of wind direction	WD_flag	
17	Rainfall	R	mm
18	Quality flag of rainfall	R_flag	
19	Upward shortwave radiation	UR	W m ⁻²
20	Quality flag of upward shortwave radiation	UR_flag	
21	Downward shortwave radiation	DR	W m ⁻²
22	Quality flag of downward shortwave radiation	DR_flag	
23	Upward longwave radiation	ULR	W m ⁻²
24	Quality flag of upward longwave radiation	ULR_flag	
25	Downward longwave radiation	DLR	W m ⁻²
26	Quality flag of downward longwave radiation	DLR_flag	
27	Water temperature at 0.2 m	T _{w_20}	°C

28	Quality flag of Water temperature at 0.2 m	T _{w_20_flag}	
29	Water temperature at 0.5 m	T _{w_50}	°C
30	Quality flag of Water temperature at 0.5 m	T _{w_50_flag}	
31	Water temperature at 1.0 m	T _{w_100}	°C
32	Quality flag of Water temperature at 1.0 m	T _{w_100_flag}	
33	Water temperature at 1.5 m	T _{w_150}	°C
34	Quality flag of water temperature at 1.5 m	T _{w_150_flag}	
35	Sediment temperature	T _{w_bot}	°C
36	Quality flag of sediment temperature	T _{w_bot_flag}	
37	Friction velocity	U*	m s ⁻¹
38	Quality flag of friction velocity	U*_flag	
39	Sensible heat flux	H	W m ⁻²
40	Quality flag of sensible heat flux	H_flag	
41	Latent heat flux	LE	W m ⁻²
42	Quality flag of latent heat flux	LE_flag	

374 Notes: 1) Time marks end of a half-hourly observation in Beijing time (UTC+8:00); 2) At the DS site,
375 columns 27, 29, and 31 represent soil temperature at 5, 10, and 20 cm, respectively, column 33 represents
376 soil heat flux G (W m⁻²) measured at 5-cm depth, and column 34 represents quality flag of soil heat flux.
377 .
378

Table 5. Uncertainty of key measurement variables at half-hourly intervals. Instrument uncertainty is provided by the manufacturers. Performance uncertainty is one standard deviation of the difference between measurements made by the field instrument and the validation instrument. Environmental uncertainty is the spatial standard deviation of the variable measured at the lake sites.

Variable	Uncertainty	Period of evaluation
Instrument uncertainty		
P	± 0.3 hPa	
Ta	± 0.2 °C	
RH	± 2 %	
WS	± 0.3 m s ⁻¹	
WD	± 3 °	
UR/DR	<5%	
ULR/DLR	<10%	
Tw	± 0.6 °C	
Performance uncertainty		
UR	± 2.1 W m ⁻²	2018.06.29 – 2018.07.08; 2018.10.06 – 2018.10.15
DR	± 8.0 W m ⁻²	2018.06.29 – 2018.07.08; 2018.10.06 – 2018.10.15
ULR	± 0.5 W m ⁻²	2018.06.29 – 2018.07.08; 2018.10.06 – 2018.10.15
DLR	± 1.3 W m ⁻²	2018.06.29 – 2018.07.08; 2018.10.06 – 2018.10.15
u*	± 0.06 m s ⁻¹	2020.7.13 – 2020.8.23
H	± 3.1 W m ⁻²	2020.7.13 – 2020.8.23
LE	± 21.2 W m ⁻²	2020.7.13 – 2020.8.23
Environmental uncertainty		
Water depth	± 0.06 m	2017.09.01 – 2018.08.31
Ta	± 0.50 °C	2018.07.01 – 2018.07.31
DR	± 36.3 W m ⁻²	2018.07.01 – 2018.07.31

Formatted: Font: Bold

Formatted Table

Formatted Table

Formatted: Superscript

Formatted: Superscript

Formatted: Superscript

Formatted: Superscript

Formatted Table

Formatted: Superscript

Formatted: Superscript

Formatted: Superscript

Formatted: Superscript

Formatted: Subscript

Formatted: Superscript

Formatted: Superscript

Formatted: Superscript

Formatted Table

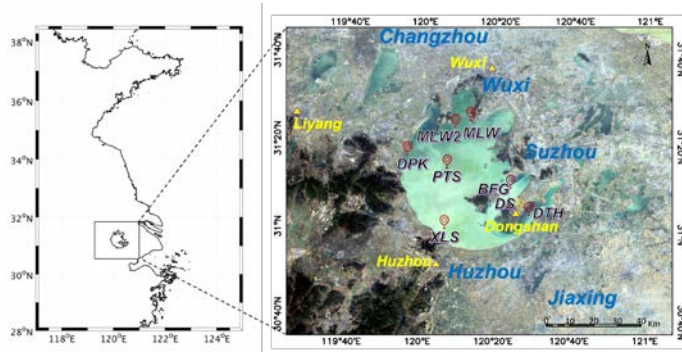
Formatted: Superscript

Formatted: Superscript

Formatted: Left

387

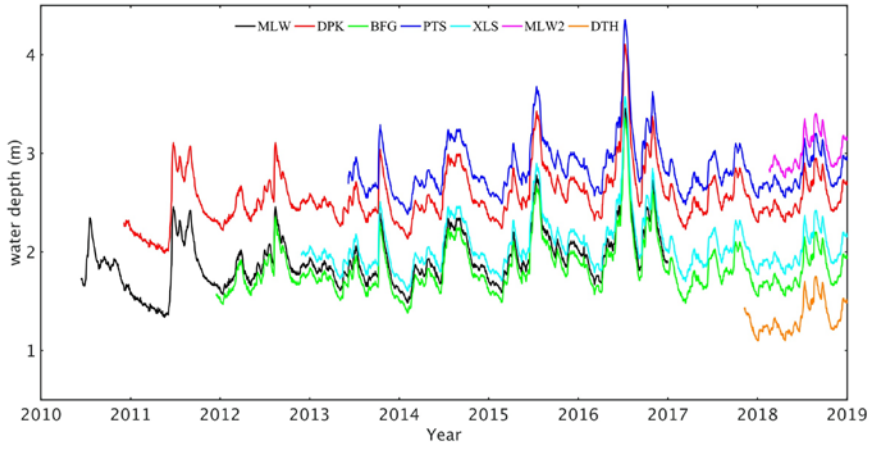
388



389

390 **Figure 1.** Map showing locations of Lake Taihu, eddy covariance sites (red bubbles) and
391 WMO weather stations (yellow triangles). City names are shown in blue. DS is a land site,
392 and MLW, MLW2, DPK, PTS, XLS, BFG and DTH are lake sites. The background is a
393 natural color image from LANDSAT 8 without correction for atmospheric interference.
394

395



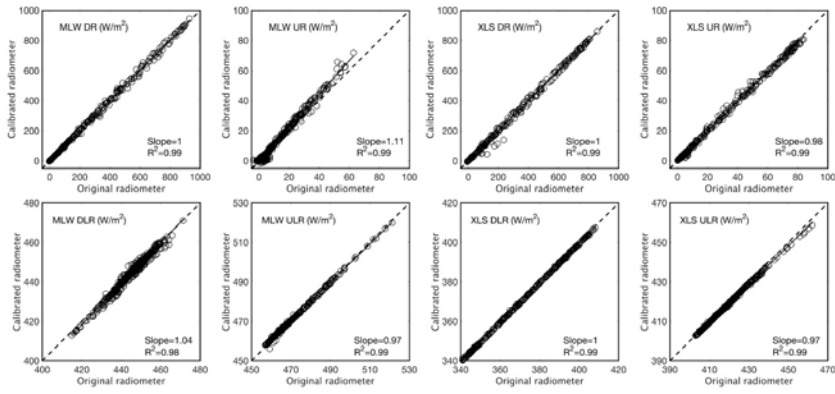
396

397 **Figure 2.** Water depth at the eddy covariance sites.

398

399

400
401
402

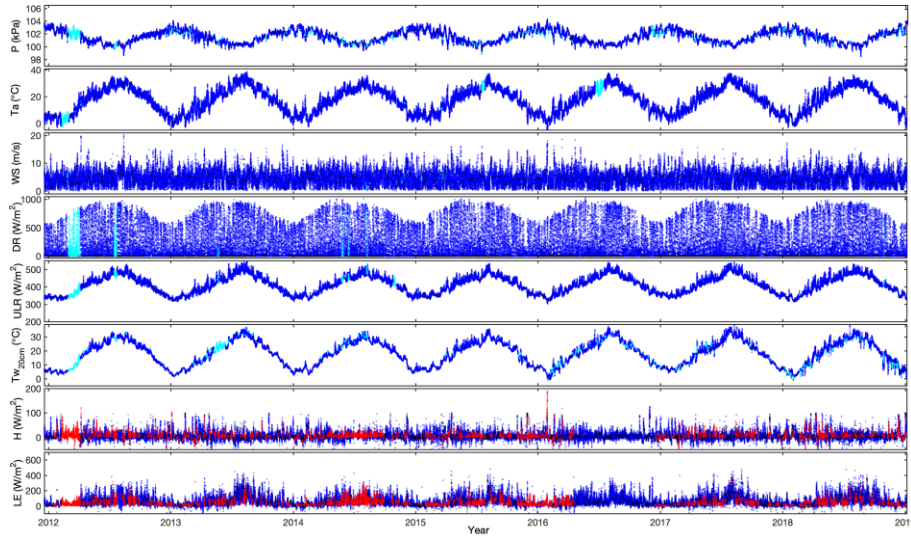


403
404 **Figure 3.** Comparison of four components of the radiation balance between the original
405 radiometer (horizontal axis) and a laboratory standard (vertical axis) at MLW and XLS. Refer
406 to Table 4 for variable definitions.

407
408

409

410



411

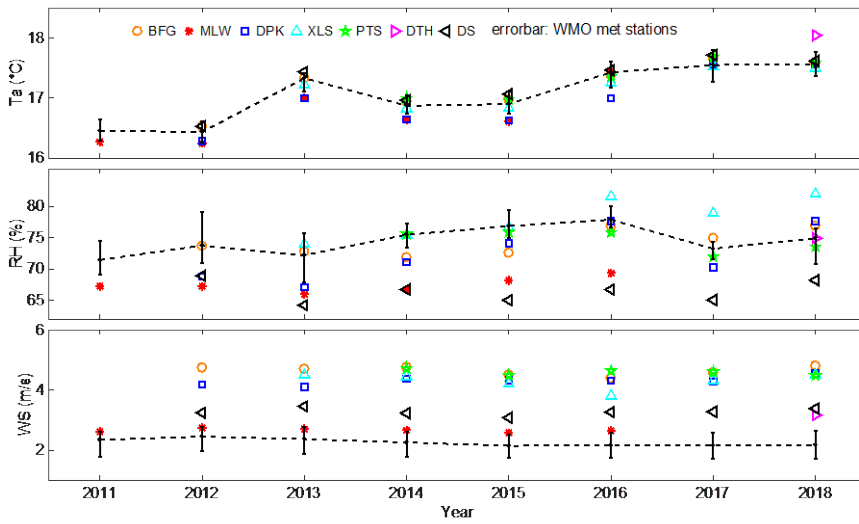
412 **Figure 4.** Complete gap-filled time series for selected variables observed at BFG. Blue, black,
413 cyan and red dots represent quality flag 0, 1, 2, and 3, respectively. Variable definitions are
414 given in Table 4

415

416

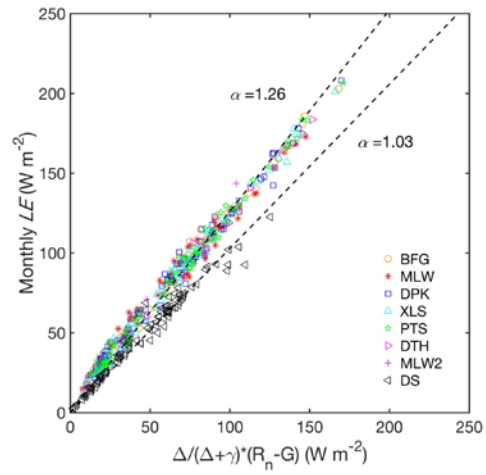
417

418
419



420
421 **Figure 5.** Annual mean air temperature (top), relative humidity (middle) and wind speed
422 (bottom) observed at the eddy flux sites (symbols) and at the four WMO weather stations
423 around the lake (line). Error bars represent the range of the annual means of the four WMO
424 stations.
425

426

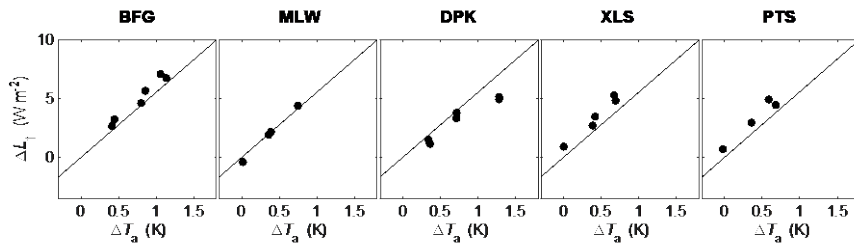


427

428

429 **Figure 6.** Comparison of observed monthly latent heat flux with Priestley-Taylor model
430 prediction using the original α coefficient of 1.26 and a modified coefficient of 1.03. Here
431 R_n is net radiation, G is heat storage in the water column, Δ is the slope of the saturation
432 vapor pressure curve, and γ is the psychrometric constant.

433



434

435 **Figure 7.** The relationship between changes in observed annual mean upward longwave
 436 radiation flux and annual mean air temperature (dots). Solid lines represent the prediction of
 437 the Stefan-Boltzmann Law.

438

439

440 **References**

- 441 Barr, A. G., King, K. M., Gillespie, T. J., Den Hartog, G. and Neumann, H. H.: A comparison of Bowen ratio
442 and eddy correlation sensible and latent heat flux measurements above deciduous forest, *Boundary-Layer
443 Meteorol.*, 71(1–2), 21–41, 1994.
- 444 Blanken, P. D., Black, T. A., Yang, P. C., Neumann, H. H., Nestic, Z., Staebler, R., Den Hartog, G., Novak, M.
445 D. and Lee, X.: Energy balance and canopy conductance of a boreal aspen forest: partitioning overstory and
446 understory components, *J. Geophys. Res. Atmos.*, 102(D24), 28915–28927, 1997.
- 447 Blanken, P. D., Spence, C., Hedstrom, N. and Lenters, J. D.: Evaporation from Lake Superior: 1. Physical
448 controls and processes, *J. Great Lakes Res.*, 37(4), 707–716, doi:10.1016/j.jglr.2011.08.009, 2011.
- 449 Charusombat, U., Fujisaki-Manome, A., Gronewold, A. D., Lofgren, B. M., Anderson, E. J., Blanken, P.,
450 Spence, C., Lenters, J. D., Xiao, C. and Fitzpatrick, L. E.: Evaluating and improving modeled turbulent heat
451 fluxes across the North American Great Lakes, *Hydrol. Earth Syst. Sci.*, 22(10), 2018.
- 452 Deng, B., Liu, S., Xiao, W., Wang, W., Jin, J. and Lee, X.: Evaluation of the CLM4 lake model at a large and
453 shallow freshwater lake, *J. Hydrometeorol.*, 14(2), 636–649, doi:10.1175/JHM-D-12-067.1, 2013.
- 454 Downing, J. A., Prairie, Y. T., Cole, J. J., Duarte, C. M., Tranvik, L. J., Striegl, R. G., McDowell, W. H.,
455 Kortelainen, P., Caraco, N. F., Melack, J. M. and Middelburg, J. J.: The global abundance and size distribution
456 of lakes, ponds, and impoundments, *Limnol. Oceanogr.*, 51(5), 2388–2397, doi:10.4319/lo.2006.51.5.2388,
457 2006.
- 458 Du, Q., Liu, H., Xu, L., Liu, Y. and Wang, L.: The monsoon effect on energy and carbon exchange processes
459 over a highland lake in the southwest of China, *Atmos. Chem. Phys.*, 18(20), 15087–15104, 2018.
- 460 Franz, D., Mammarella, I., Boike, J., Kirillin, G., Vesala, T., Bornemann, N., Larmanou, E., Langer, M. and
461 Sachs, T.: Lake-atmosphere heat flux dynamics of a thermokarst lake in arctic Siberia, *J. Geophys. Res. Atmos.*,
462 123(10), 5222–5239, 2018.
- 463 Franz, D., Mammarella, I., Boike, J., Kirillin, G., Vesala, T., Bornemann, N., Larmanou, E., Langer, M. and
464 Sachs, T.: Lake-atmosphere heat flux dynamics of a thermokarst lake in arctic Siberia, *J. Geophys. Res. Atmos.*,
465 123(10), 5222–5239, 2018.
- 466 Hamdani, I., Assouline, S., Tanny, J., Lensky, I. M., Gertman, I., Mor, Z. and Lensky, N. G.: Seasonal and
467 diurnal evaporation from a deep hypersaline lake: the Dead Sea as a case study, *J. Hydrol.*, 562, 155–167, 2018.
- 468 Hu, C., Wang, Y., Wang, W., Liu, S., Piao, M., Xiao, W. and Lee, X.: Trends in evaporation of a large
469 subtropical lake, *Theor. Appl. Climatol.*, 129(1–2), 159–170, doi:10.1007/s00704-016-1768-z, 2017.
- 470 Lee, X., Massman, W. and Law, B.: *Handbook of micrometeorology: a guide for surface flux measurement and
471 analysis*, Springer Science & Business Media., 2004.

472 Lee, X., Liu, S., Xiao, W., Wang, W., Gao, Z., Cao, C., Hu, C., Hu, Z., Shen, S., Wang, Y., Wen, X., Xiao, Q.,
473 Xu, J., Yang, J. and Zhang, M.: The taihu eddy flux network: An observational program on energy, water, and
474 greenhouse gas fluxes of a large freshwater lake, *Bull. Am. Meteorol. Soc.*, 95(10), 1583–1594,
475 doi:10.1175/BAMS-D-13-00136.1, 2014.

476 Li, Z., Lyu, S., Ao, Y., Wen, L., Zhao, L. and Wang, S.: Long-term energy flux and radiation balance
477 observations over Lake Ngoring, Tibetan Plateau, *Atmos. Res.*, 155, 13–25, 2015.

478 Nordbo, A., Launiainen, S., Mammarella, I., Leppäranta, M., Huotari, J., Ojala, A. and Vesala, T.: Long-term
479 energy flux measurements and energy balance over a small boreal lake using eddy covariance technique, *J.*
480 *Geophys. Res. Atmos.*, 116(D2), 2011.

481 Subin, Z. M., Riley, W. J. and Mironov, D.: An improved lake model for climate simulations: Model structure,
482 evaluation, and sensitivity analyses in CESM1, *J. Adv. Model. Earth Syst.*, 4(2), 1–27,
483 doi:10.1029/2011MS000072, 2012.

484 Tanny, J., Cohen, S., Assouline, S., Lange, F., Grava, A., Berger, D., Teltch, B. and Parlange, M. B.:
485 Evaporation from a small water reservoir: Direct measurements and estimates, *J. Hydrol.*, 351(1–2), 218–229,
486 2008.

487 Twine, T. E., Kustas, W. P., Norman, J. M., Cook, D. R., Houser, Pr., Meyers, T. P., Prueger, J. H., Starks, P. J.
488 and Wesely, M. L.: Correcting eddy-covariance flux underestimates over a grassland, *Agric. For. Meteorol.*,
489 103(3), 279–300, 2000.

490 Verpoorter, C., Kutser, T., Seekell, D. A. and Tranvik, L. J.: A global inventory of lakes based on
491 high-resolution satellite imagery, *Geophys. Res. Lett.*, 41(18), 6396–6402, doi:10.1002/2014GL060641, 2014.

492 Vesala, T., Huotari, J., Rannik, Ü., Suni, T., Smolander, S., Sogachev, A., Launiainen, S. and Ojala, A.: Eddy
493 covariance measurements of carbon exchange and latent and sensible heat fluxes over a boreal lake for a full
494 open-water period, *J. Geophys. Res. Atmos.*, 111(11), 1–12, doi:10.1029/2005JD006365, 2006.

495 Wang, B., Ma, Y., Wang, Y., Su, Z. and Ma, W.: Significant differences exist in lake-atmosphere interactions
496 and the evaporation rates of high-elevation small and large lakes, *J. Hydrol.*, 573, 220–234, 2019.

497 Wang, W., Xiao, W., Cao, C., Gao, Z., Hu, Z., Liu, S., Shen, S., Wang, L., Xiao, Q., Xu, J., Yang, D. and Lee,
498 X.: Temporal and spatial variations in radiation and energy balance across a large freshwater lake in China, *J.*
499 *Hydrol.*, 511, 811–824, doi:10.1016/j.jhydrol.2014.02.012, 2014.

500 Wang, Y., Gao, Y., Qin, H., Huang, J., Liu, C., Hu, C., Wang, W., Liu, S. and Lee, X.: Spatiotemporal
501 Characteristics of Lake Breezes over Lake Taihu, China, *J. Appl. Meteorol. Climatol.*, 56(7), 2053–2065, 2017.

502 Webb, E. K., Pearman, G. I. and Leuning, R.: Correction of flux measurements for density effects due to heat
503 and water vapour transfer, *Q. J. R. Meteorol. Soc.*, 106(447), 85–100, 1980.

504 Wilson, K., Goldstein, A., Falge, E., Aubinet, M., Baldocchi, D., Berbigier, P., Bernhofer, C., Ceulemans, R.,

505 Dolman, H. and Field, C.: Energy balance closure at FLUXNET sites, *Agric. For. Meteorol.*, 113(1–4), 223–243,
506 2002.

507 Xiao, K., Griffis, T. J., Baker, J. M., Bolstad, P. V., Erickson, M. D., Lee, X., Wood, J. D., Hu, C. and Nieber, J.
508 L.: Evaporation from a temperate closed-basin lake and its impact on present, past, and future water level, *J.*
509 *Hydrol.*, 561, 59–75, 2018.

510 Xiao, W., Liu, S., Wang, W., Yang, D., Xu, J., Cao, C., Li, H. and Lee, X.: Transfer Coefficients of Momentum,
511 Heat and Water Vapour in the Atmospheric Surface Layer of a Large Freshwater Lake, *Boundary-Layer*
512 *Meteorol.*, 148(3), 479–494, doi:10.1007/s10546-013-9827-9, 2013.

513 Xiao, W., Liu, S., Li, H., Xiao, Q., Wang, W., Hu, Z., Hu, C., Gao, Y., Shen, J., Zhao, X., Zhang, M. and Lee,
514 X.: A flux-gradient system for simultaneous measurement of the CH₄, CO₂, and H₂O fluxes at a lake-air
515 interface, *Environ. Sci. Technol.*, 48(24), 14490–14498, doi:10.1021/es5033713, 2014.

516 Xu, J., Lee, X., Xiao, W., Cao, C., Liu, S., Wen, X., Xu, J., Zhang, Z. and Zhao, J.: Interpreting the ¹³C/¹²C ratio
517 of carbon dioxide in an urban airshed in the Yangtze River Delta, China, *Atmos. Chem. Phys.*, 17(5),
518 doi:10.5194/acp-17-3385-2017, 2017.

519 Yusup, Y. and Liu, H.: Effects of Atmospheric Surface Layer Stability on Turbulent Fluxes of Heat and Water
520 Vapor across the Water–Atmosphere Interface, *J. Hydrometeorol.*, 17(11), 2835–2851, 2016.

521 Zhang, M., Xiao, Q., Zhang, Z., Gao, Y., Zhao, J., Pu, Y., Wang, W., Xiao, W., Liu, S. and Lee, X.: Methane
522 flux dynamics in a submerged aquatic vegetation zone in a subtropical lake, *Sci. Total Environ.*, 672,
523 doi:10.1016/j.scitotenv.2019.03.466, 2019a.

524 Zhang, X., Huang, J., Li, G., Wang, Y., Liu, C., Zhao, K., Tao, X., Hu, X.-M. and Lee, X.: Improving
525 Lake-Breeze Simulation with WRF Nested LES and Lake Model over a Large Shallow Lake, *J. Appl. Meteorol.*
526 *Climatol.*, 58(8), 1689–1708, 2019b.

527 Zhang, Z., Zhang, M., Cao, C., Wang, W., Xiao, W., Xie, C., Chu, H., Wang, J., Zhao, J., Jia, L., Liu, Q.,
528 Huang, W., Zhang, W., Lu, Y., Xie, Y., Wang, Y., Pu, Y., Hu, Y., Chen, Z., Qin, Z. and Lee, X.: A dataset of
529 microclimate and radiation and energy fluxes from the Lake Taihu Eddy Flux Network, Harvard Dataverse,
530 <https://doi.org/10.7910/DVN/HEWCWM>, 2020

531 Zhao, X. and Liu, Y.: Variability of surface heat fluxes and its driving forces at different time scales over a large
532 ephemeral lake in China, *J. Geophys. Res. Atmos.*, 123(10), 4939–4957, 2018.

533